

A Sino-German $\lambda 6$ cm polarization survey of the Galactic plane

VII. Small supernova remnants

X. H. Sun^{1,2}, P. Reich², W. Reich², L. Xiao¹, X. Y. Gao¹, and J. L. Han¹

¹ National Astronomical Observatories, CAS, Jia-20 Datun Road, Chaoyang District, Beijing 100012, China
e-mail: [xhsun;hj1]@nao.cas.cn

² Max-Planck-Institut für Radioastronomie, Auf dem Hügel 69, 53121 Bonn, Germany
e-mail: [preich;wreich]@mpifr-bonn.mpg.de

Received / Accepted

ABSTRACT

Aims. We study the spectral and polarization properties of supernova remnants (SNRs) based on our $\lambda 6$ cm survey data.

Methods. The observations were taken from the Sino-German $\lambda 6$ cm polarization survey of the Galactic plane. By using the integrated flux densities at $\lambda 6$ cm together with measurements at other wavelengths from the literature we derive the global spectra of 50 SNRs. In addition, we use the observations at $\lambda 6$ cm to present the polarization images of 24 SNRs.

Results. We derived integrated flux densities at $\lambda 6$ cm for 51 small SNRs with angular sizes less than 1° . Global radio spectral indices were obtained in all the cases except for Cas A. For SNRs G15.1–1.6, G16.2–2.7, G16.4–0.5, G17.4–2.3, G17.8–2.6, G20.4+0.1, G36.6+2.6, G43.9+1.6, G53.6–2.2, G55.7+3.4, G59.8+1.2, G68.6–1.2, and G113.0+0.2, the spectra have been significantly improved. From our analysis we argue that the object G16.8–1.1 is probably an H II region instead of a SNR. Cas A shows a secular decrease in total intensity, and we measured a flux density of 688 ± 35 Jy at $\lambda 6$ cm between 2004 and 2008. Polarized emission from 25 SNRs were detected. For G16.2–2.7, G69.7+1.0, G84.2–0.8 and G85.9–0.6, the polarized emission is detected for the first time confirming them as SNRs.

Conclusions. High frequency observations of SNRs are rare but important to establish their spectra and trace them in polarization in particular towards the inner Galaxy where Faraday effects are important.

Key words. ISM: supernova remnants – Surveys – Polarization – Radio continuum: general – Methods: observational

1. Introduction

Supernovae release enormous energy into the interstellar medium (ISM). The ejected material as well as the material swept up by the shock wave form the supernova remnants (SNRs). SNRs can be traced up to several ten-thousand years (e.g. Reich 2002, for a review). To study the evolution of SNRs is a key to understand the interaction between the blast wave from the supernova explosion and the ISM. Since SNRs are primary radio objects, the morphology, spectrum, and magnetic field configuration obtained from radio observations provide vital input to figure out the evolution of SNRs.

The Sino-German $\lambda 6$ cm polarization survey of the Galactic plane covers the broad band of the Galactic plane of $10^\circ \leq l \leq 230^\circ$ and $|b| \leq 5^\circ$ (Sun et al. 2007; Gao et al. 2010; Sun et al. 2011; Xiao et al. 2011). The polarization structures such as Faraday screens, voids and canals revealed in the survey have advanced the understanding of the ISM. Meanwhile many SNRs were detected as strong discrete sources in the survey. A study of large SNRs with angular sizes exceeding about 1° was already presented by Gao et al. (2011). In this paper, we focus on SNRs with a smaller angular size. Most of these small SNRs cannot be resolved in the survey, so that we could not investigate their morphology in detail. We obtained their integrated flux densities and established their spectra together with data at other radio wavelengths. Although spectra for most of the SNRs have already been presented in the literature, we are able to make significant improvements particularly for some weak and slightly

extended SNRs by using the new measured flux densities from the $\lambda 6$ cm and the Effelsberg $\lambda 11$ cm and $\lambda 21$ cm surveys (Reich et al. 1990a; Fürst et al. 1990; Reich et al. 1990b, 1997). We also obtained polarization images for about half of the SNRs, some of which were used to estimate rotation measures (RMs) in context with polarization data obtained at other wavelengths such as $\lambda 11$ cm and $\lambda 2.8$ cm.

The paper is organized as follows: We briefly describe the $\lambda 6$ cm survey in Sect. 2. The results are reported in Sect. 3, where the integrated flux densities and spectra of 50 SNRs are presented, the polarization images of 24 SNRs are displayed, and a possible mis-identification of G16.8–1.1 is discussed. Due to the secular decrease in intensity of Cas A, this remnant is studied separately. The summary is given in Sect. 4.

2. The $\lambda 6$ cm survey

The Sino-German $\lambda 6$ cm polarization survey of the Galactic plane has been conducted by using the Urumqi 25-m telescope located about 70 km south of Urumqi city with the geographic longitude of 87°E and latitude of $+43^\circ$. The survey has an angular resolution of $9.5''$ and a system temperature of about 22 K towards the zenith. The central frequency was set to either 4.8 GHz or 4.963 GHz with corresponding bandwidths of 600 MHz and 295 MHz. The system gain is $T_B[\text{K}]/S[\text{Jy}] = 0.164$. Detailed information about the receiving system was already presented by Sun et al. (2007).

The Galactic plane was mapped in raster scans in both longitude and latitude directions. The separation of sub-scans was $3'$, and the scan velocity was $4^\circ/\text{min}$. Observations were made at night time with clear sky. The primary calibrator was 3C 286 with an assumed flux density at $\lambda 6$ cm $S_{6\text{cm}} = 7.5$ Jy consistent with that by Baars et al. (1977), a polarization percentage of 11.3%, and a polarization angle $\text{PA} = 33^\circ$. The sources 3C 48 and 3C 138 were used as secondary calibrators, and 3C 295 and 3C 147 as unpolarized calibrators.

The raw data from the receiving system contain maps of I , U , and Q stored in NOD2-format (Haslam 1974). Data processing follows the standard procedures developed for continuum observations with the Effelsberg 100-m telescope as detailed by Sun et al. (2007) and Gao et al. (2010). In the final maps, the typical rms noise level is about 1 mK T_B for total intensity I , and 0.5 mK T_B for Stokes U and Q , and polarized intensity (PI).

3. Results

According to Green's catalogue¹ (Green 2009), there are 99 small SNRs with angular sizes less than 1° in the survey region. Most of them are smaller than about $30'$ in size. A large fraction (80%) of these SNRs is located in the region of $10^\circ < l < 60^\circ$, where the diffuse emission is the strongest (Sun et al. 2011). Because of strong confusion along the Galactic plane, it is difficult to determine flux densities of some of these SNRs. Patchy structures dominate the polarization images (Sun et al. 2011; Xiao et al. 2011), which makes it even more challenging to extract polarization information intrinsic to these SNRs. As it is shown in Sect. 3.1, we managed to obtain integrated flux densities for 51 SNRs and polarization images of 24 SNRs.

The SNR G111.7–2.1 (Cas A) is presently the brightest source beyond the solar system in the sky. Cas A is known to decrease in intensity by a measurable amount every year. Therefore we discuss this object separately.

3.1. Integrated flux densities

To determine integrated flux densities of the SNRs, we first removed the large-scale diffuse emission using the “background filtering” technique developed by Sofue & Reich (1979). The filter beam size was set to about two or three times of the source size, to ensure that no emission from the SNR is eliminated. We then made integrations within a polygon region encompassing the SNR and subtracted the background estimated by averaging the intensities surrounding the edge areas of the SNR. If the SNR had a size comparable to the beam, we made a two-dimensional elliptical Gaussian fit to assess the flux density. For large circular objects, we performed a ring integration of the emission to calculate the total flux density.

We were able to measure the $\lambda 6$ cm integrated flux densities of 51 SNRs. Among the remaining SNRs, some objects, such as G11.0–0.0, could not be separated from the strong emission along the plane. Emission from other objects, such as G83.0–0.3, was mixed up with the strong thermal emission from the Cygnus region, and some SNRs, such as G54.4–0.3 (HC 40), are located in a complicated environment and their boundaries could not be well defined. For all these objects we could not determine their flux densities with sufficient precision.

Flux densities at $\lambda 6$ cm for 50 SNRs, excluding Cas A, are listed in the fourth column of Table 1. For comparison,

previous measurements at $\lambda 6$ cm and the corresponding references are listed in the second and third column, respectively. In case that there are several flux density measurements at $\lambda 6$ cm published, we selected the one with the highest quality. If the qualities are comparable we used the median. The early measured flux densities have been corrected to conform to the scale by Baars et al. (1977). Some of the corrections were provided by Kassim (1989b). The new measurements generally are in good agreement, within uncertainties, with previous published values. For 17 SNRs: G15.1–1.6, G15.4+0.1, G16.2–2.7, G16.4–0.5, G17.4–2.3, G17.8–2.6, G20.4+0.1, G36.6+2.6, G40.5–0.5, G43.9+1.6, G53.6–2.2 (3C 400.2), G55.7+3.4, G59.8+1.2, G68.6–1.2, G96.0+2.0, G109.1–1.0 (CTB 109), and G113.0+0.2, no $\lambda 6$ cm flux densities have been obtained up to date.

3.2. SNR spectra

We calculated the spectral indices of these SNRs by fitting flux densities from the literature together with the new measurements at $\lambda 6$ cm versus frequencies in logarithmic scale with weighted least squares. Some published flux densities could not be corrected to the scale by Baars et al. (1977) because no calibration information could be found, which has only slight influence to the spectra. The newly obtained spectral indices for which we used additional published data with references in the eighth column, are listed in the seventh column in Table 1. We did not include data below 100 MHz to investigate the low-frequency spectrum turnover (e.g. Kassim 1989a), as we are only interested in the high-frequency spectrum, which the new $\lambda 6$ cm measurements can help to establish. For comparison, previous indices and corresponding references are listed in the fifth and sixth column in Table 1. If a spectral break in a SNR spectrum was firmly established, the spectral indices below and above the turnover frequency are both provided. New integrated flux densities at $\lambda 11$ cm and $\lambda 21$ cm were also derived in case either no flux density measurements were found or the data available in the literature were not sufficient to constrain the spectra. Unless otherwise noted, the flux densities at these two bands were measured from the $\lambda 11$ cm and $\lambda 21$ cm Effelsberg surveys² (Reich et al. 1990a; Fürst et al. 1990; Reich et al. 1990b, 1997). The angular resolution and sensitivity are 4.3 and 20 mK for the $\lambda 11$ cm survey, and 9.4 and 40 mK for the $\lambda 21$ cm survey. Both surveys have total intensity scales consistent with that by Baars et al. (1977). The reference entry (Column 8 in Table 1) remains empty if no earlier measurements were available. Plots of all SNR spectra are shown in Fig. 1.

For nearly half of the SNRs in Fig. 1, the new $\lambda 6$ cm measurements are the only or amongst the highest frequency data, and are therefore important to constrain the high-frequency spectra. These SNRs are: G11.1–1.0, G15.1–1.6, G15.4+0.1, G15.9+0.2, G16.2–2.7, G16.4–0.5, G16.7+0.1, G17.4–2.3, G17.8–2.6, G20.0–0.2, G20.4+0.1, G36.6+2.6, G43.9+1.6, G53.6–2.2, G55.7+3.4, G59.8+1.2, G68.6–1.2, G69.7+1.0, G94.0+1.0, G96.0+2.0, G113.0+0.2, and G116.9+0.2.

For 13 SNRs, improved spectra have been determined by combining the flux densities at $\lambda 6$ cm, $\lambda 11$ cm, and $\lambda 21$ cm, which are further proved by the TT-plot (Turtle et al. 1962) results (see for example Fig. 2). The relation $\alpha = \beta + 2$ is used to convert the spectral index β from TT-plot into α . These SNRs are: G15.1–1.6, G16.2–2.7, G16.4–0.5, G17.4–2.3, G17.8–2.6,

¹ The Catalog of Galactic Supernova Remnants is available at the web site <http://www.mrao.cam.ac.uk/surveys/snrs>

² The data are available in the “Survey Sampler” maintained by MPIfR at the web site http://www.mpifr.de/old_mpifr/survey.html

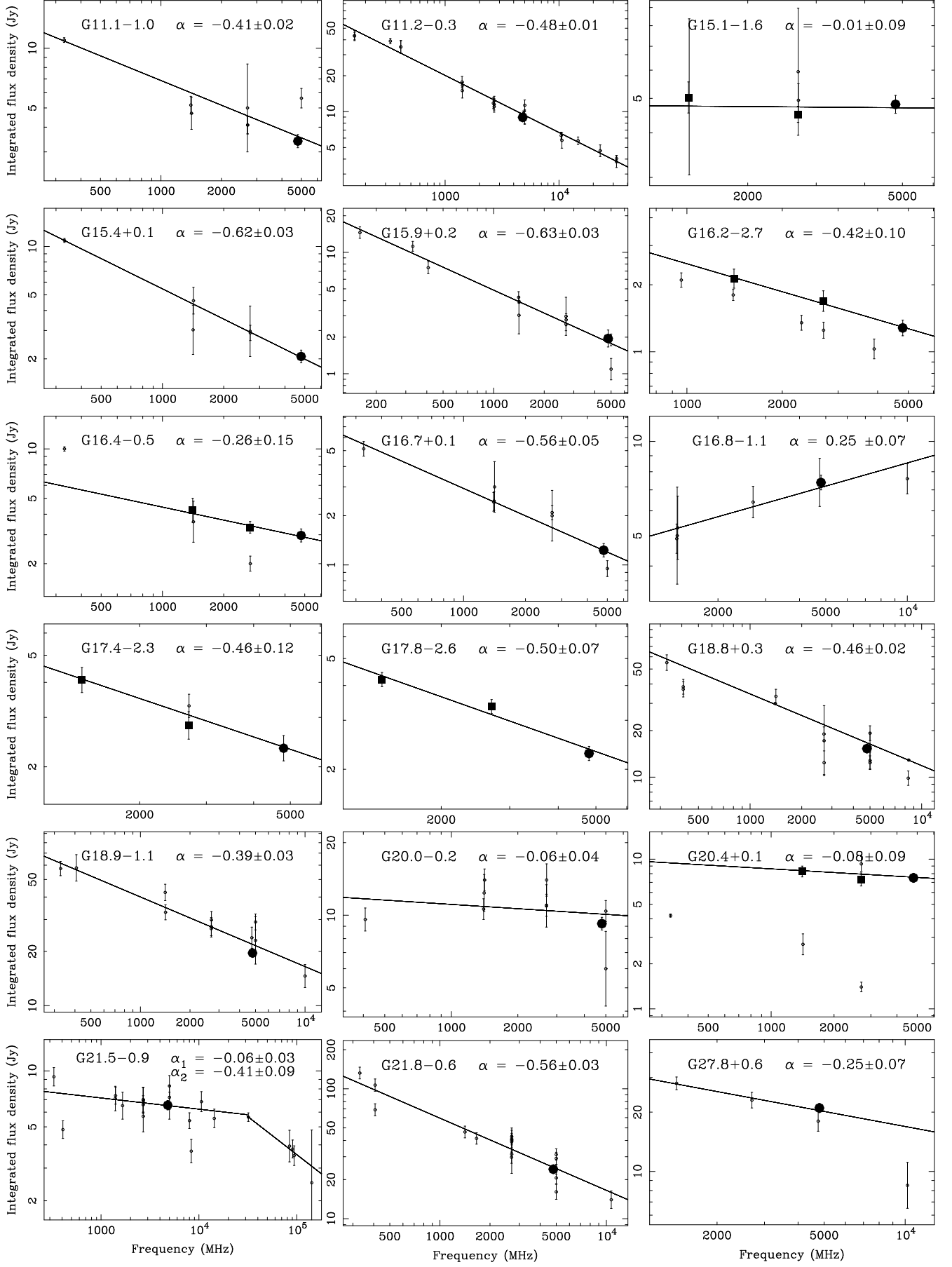


Fig. 1. Spectra for 50 SNRs. The present $\lambda 6$ cm flux densities are indicated by black dots, while the flux densities we derived from the $\lambda 11$ cm and $\lambda 21$ cm Effelsberg surveys are marked by dark squares. Other measurements were taken from the references listed in Table 1.

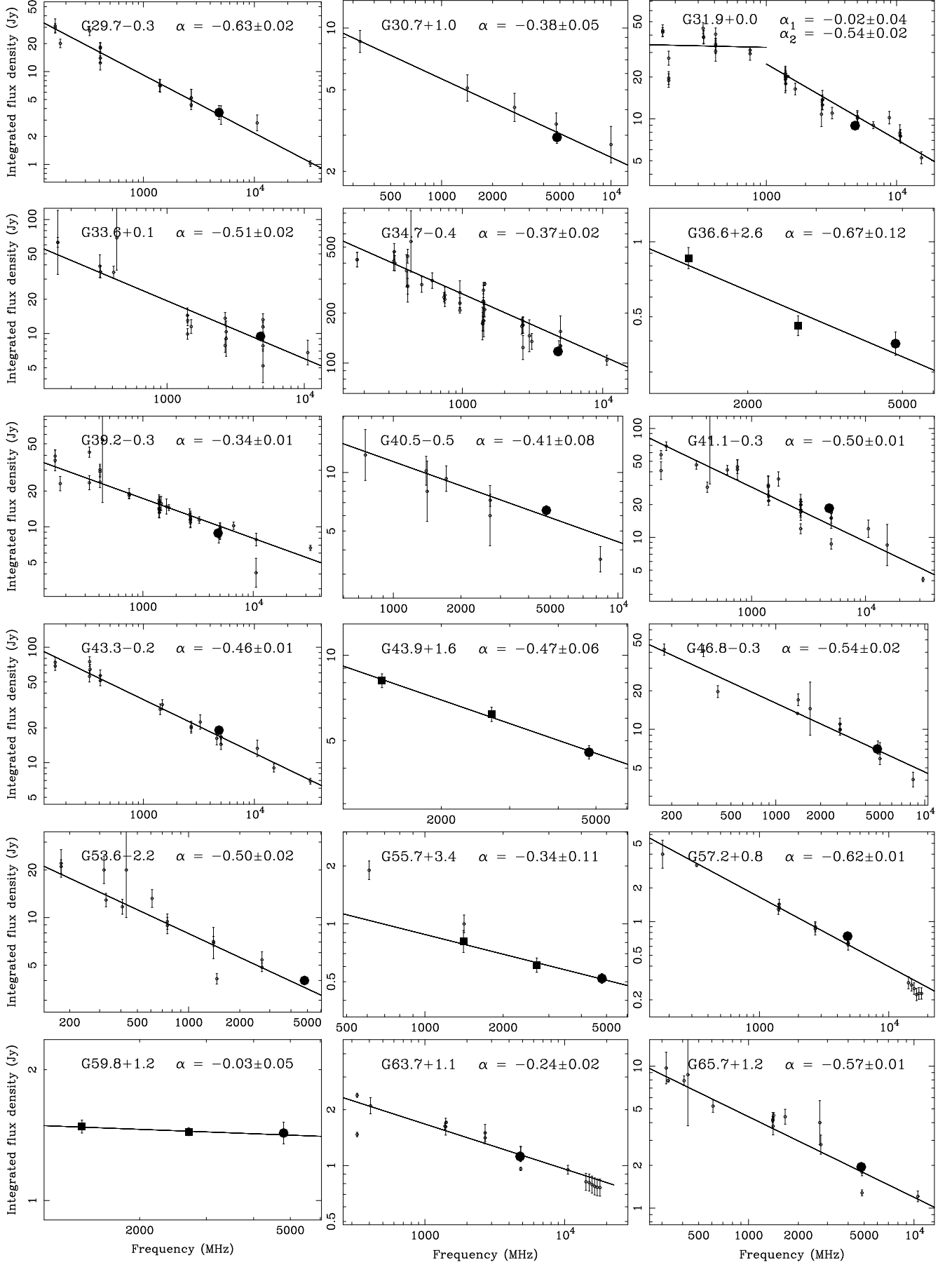


Fig. 1. –continued.

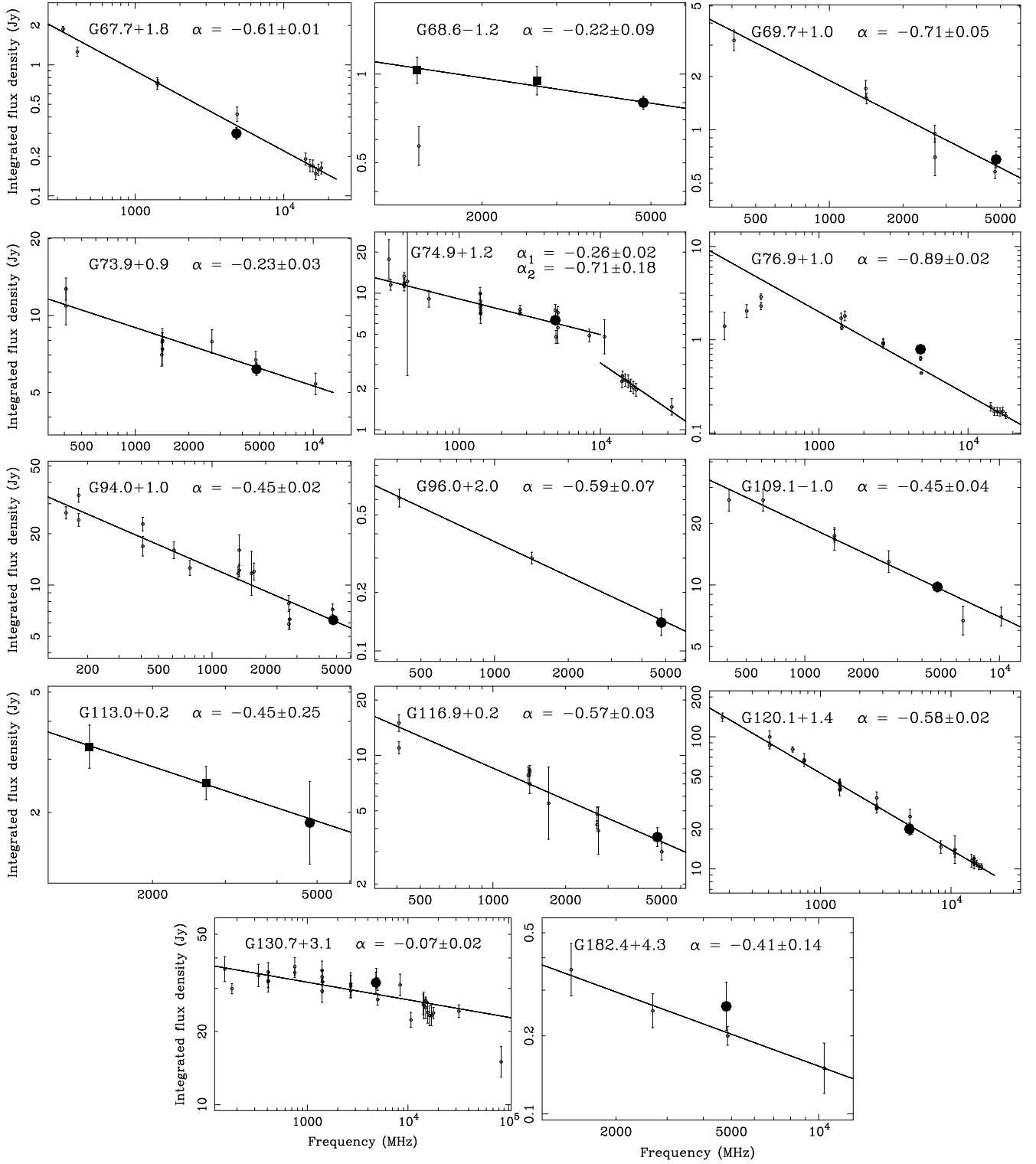


Fig. 1. –continued.

G20.4+0.1, G36.6+2.6, G43.9+1.6, G53.6–2.2, G55.7+3.4, G59.8+1.2, G68.6–1.2, and G113.0+0.2. For some of these SNRs the early measurements were not used for spectral fitting, because they, as outliers, largely deviate from the spectra based on the new data at $\lambda 6$ cm, $\lambda 11$ cm, and $\lambda 21$ cm, e.g. the measurements of G16.2–2.7 by Trushkin (1999), of G16.4–0.5 and G20.4+0.1 by Brogan et al. (2006), of G55.7+3.4 by Goss et al. (1977), and of G68.6–1.2 by Kothes et al. (2006). The reason

for the inconsistency is unclear. The spectra obtained by us are more reliable as they agree with the results from TT-plots.

For three SNRs, G21.5–0.9, G31.9+0.0 (3C 391), and G74.9+1.2 (CTB 87), the spectral turnover at high frequencies can be confirmed. The spectral break above 32 GHz for G21.5–0.9 was suggested by Salter et al. (1989b). Below 32 GHz, the spectrum is very flat with a spectral index of $\alpha = -0.06 \pm 0.03$, consistent with that given by Morsi & Reich (1987a). Above 32 GHz, the spectral index is $\alpha = -0.41 \pm 0.09$.

The spectral break for 3C 391 was noted by Moffett & Reynolds (1994a). Above 1 GHz, the spectral index of $\alpha = -0.54 \pm 0.02$ is consistent with that by Moffett & Reynolds (1994a). Below 1 GHz the spectral index is $\alpha = -0.02 \pm 0.04$. Brogan et al. (2005) ascribed the spectral turnover to absorption and obtained an opacity of 1.1 at 74 MHz, which needs confirmation at even lower frequencies. The spectral break above 11 GHz for CTB 87 was reported by Morsi & Reich (1987a) according to their 32 GHz measurement. Below 11 GHz, the spectral index obtained by Morsi & Reich (1987a) is $\alpha = -0.26$, which is consistent with our result. Adding new flux densities at 10.35 GHz (Langston et al. 2000) and 16 GHz (Hurley-Walker et al. 2009) confirms the spectral break with a spectral index of $\alpha = -0.71 \pm 0.18$ above 11 GHz. The frequency turnover for G27.8+0.6 and G130.7+3.1 is less certain and needs more high-frequency observations for confirmation.

Some SNRs, such as G15.1–1.6, G20.4+0.1, and G59.8+1.2 are probably new plerions as they have very flat spectra of $\alpha = -0.01 \pm 0.09$, $\alpha = -0.08 \pm 0.09$, and $\alpha = -0.03 \pm 0.05$. G16.8–1.1 seems misidentified and is likely an HII region as discussed below. The spectral index β from the TT-plots is the weighted average of the spectral indices from two pairs: $\lambda 6$ cm and $\lambda 11$ cm, and $\lambda 6$ cm and $\lambda 21$ cm. We comment below on those SNRs for which the newly determined spectral indices deviate by more than $3 \times \sigma$ from earlier results or when the previous spectrum was very uncertain as indicated by the question mark in Table 1.

- G11.1–1.0. Brogan et al. (2006) obtained a spectral index of $\alpha = -0.5$ between $\lambda 90$ cm and $\lambda 11$ cm data and $\alpha = -0.6$ between $\lambda 90$ cm and $\lambda 20$ cm measurements. A fit of the three data points by Brogan et al. (2006) yields a spectral index of $\alpha = -0.48 \pm 0.05$, consistent with our result of $\alpha = -0.41 \pm 0.02$.
- G15.1–1.6. The spectral index of $\alpha = -0.8$ obtained by Reich et al. (1988) is very uncertain as it was based on data only at two frequencies. We obtained a spectral index of $\alpha = -0.01 \pm 0.09$, which is that of a thermal source. However, Boumis et al. (2008) made optical observations, which convincingly showed that G15.1–1.6 is a SNR.
- G17.4–2.3. The spectral index $\alpha = -0.46 \pm 0.12$ was obtained by fitting the new flux densities at $\lambda 6$ cm, $\lambda 11$ cm, and $\lambda 21$ cm. This result is consistent with the average value $\alpha = -0.52 \pm 0.03$ using the TT-plot method.
- G17.8–2.6. With the new flux densities at $\lambda 6$ cm, $\lambda 11$ cm, and $\lambda 21$ cm we obtained a spectral index $\alpha = -0.50 \pm 0.07$, which is in good agreement with the value $\alpha = -0.52 \pm 0.13$ derived from TT-plots (Fig. 2).
- G20.4+0.1. The VLA flux densities presented by Brogan et al. (2006) (included in Fig. 1) are significantly lower than the flux densities we derived from single-dish observations. The spectrum presented here, which is characterized by $\alpha = -0.08 \pm 0.09$ and based on new flux densities at $\lambda 6$ cm, $\lambda 11$ cm, and $\lambda 21$ cm, is significantly flatter than the value $\alpha = -0.4$ reported by Brogan et al. (2006). The average spectral index derived from TT-plots among the three bands is $\alpha = -0.09 \pm 0.04$, which agrees with the integrated flux density spectrum displayed in Fig. 1.
- G36.6+2.6. The spectral index $\alpha = -0.67 \pm 0.12$ was obtained from the new flux density values at $\lambda 6$ cm, $\lambda 11$ cm, and $\lambda 21$ cm only.
- G43.9+1.6. The spectral index reported by Reich et al. (1988) is indicated as very uncertain. We derived a value $\alpha = -0.47 \pm 0.06$ from the integrated flux densities. The av-

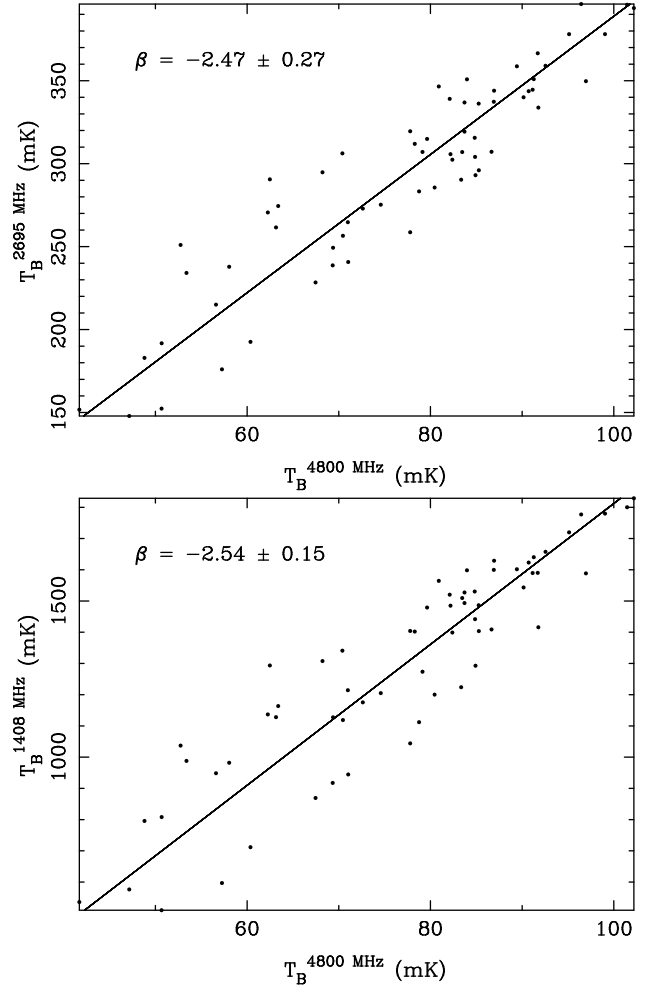


Fig. 2. TT-plots of G17.8–2.6 between $\lambda 6$ cm (4800 MHz) and $\lambda 11$ cm (2695 MHz), and between $\lambda 6$ cm and $\lambda 21$ cm (1408 MHz).

erage spectral index $\alpha = 0.59 \pm 0.10$ from TT-plots between the Urumqi $\lambda 6$ cm and the Effelsberg $\lambda 11$ cm and $\lambda 21$ cm data is consistent with the spectrum shown in Fig. 1.

- G53.6–2.2 (3C 400.2). The published spectral index $\alpha = -0.76$ listed in Table 1 results from the low VLA flux density at 1465 MHz by Dubner et al. (1994). The derived spectral index in the current work is $\alpha = -0.50 \pm 0.02$ after including the higher single-dish $\lambda 21$ cm flux density from the Effelsberg survey.
- G57.2+0.8 (4C 21.53). The derived value $\alpha = -0.62 \pm 0.01$ is slightly larger than $\alpha = -0.67$ by Hurley-Walker et al. (2009), which could be ascribed to a higher $\lambda 6$ cm flux density.
- G59.8+1.2. This SNR was found to have a flat spectrum rather than a steep spectrum as it was reported earlier by Reich et al. (1988). Optical observations by Boumis et al. (2005) showed a large SII/H α ratio, which confirms this source as non-thermal. It may be classified as a pulsar wind nebula (PWN) instead of a classical shell-type SNR. This object consists of an elliptically shaped source and a tail. Based on TT-plots we obtained spectral indices of $\alpha = -0.13 \pm 0.06$ between $\lambda 6$ cm and $\lambda 11$ cm and $\alpha = -0.03 \pm 0.10$ between $\lambda 6$ cm and $\lambda 21$ cm for the source component. Their weighted average spectral index is $\alpha = -0.09 \pm 0.05$, almost consistent with $\alpha = -0.03 \pm 0.05$ from integrated flux densities as shown

in Fig. 1. The spectral index does not change when including the tail. Unfortunately no polarized emission is visible in the $\lambda 6$ cm maps. There is no ROSAT X-ray emission associated, and no pulsar reported so far is in the direction of G59.8+1.2. More detailed investigations are required to firmly establish its classification.

- G68.6–1.2. This SNR was discovered by Reich et al. (1988). Based on the new flux densities at $\lambda 6$ cm, $\lambda 11$ cm, and $\lambda 21$ cm we derived a spectral index $\alpha = -0.22 \pm 0.09$. The $\lambda 21$ cm flux density quoted by Kothes et al. (2006) was not included in the fit, as it largely deviates from the spectrum.
- G76.9+1.0. This object strongly resembles the PWN DA 495 (Landecker et al. 1993). Available flux densities indicate a spectral turnover at about 1 GHz. Fitting the measurements above 1 GHz and including the new data at 16 GHz by Hurley-Walker et al. (2009) we obtained a spectral index $\alpha = -0.89 \pm 0.02$. This steepening probably stems from synchrotron aging similar to what is seen in DA 495 (Kothes et al. 2008).
- G113.0+0.2. This SNR with strong polarized emission was discovered by Kothes et al. (2005). However, so far no flux density could be quoted as it is a very weak and extended SNR. Besides the flux density at $\lambda 6$ cm, we also measured its flux density at $\lambda 11$ cm and $\lambda 21$ cm from the Effelsberg surveys. The spectral index is $\alpha = -0.45 \pm 0.25$ supported by the TT-plot result of $\alpha = -0.43 \pm 0.12$.

3.3. Polarization

The “background filtering” method (Sofue & Reich 1979) cannot be used to remove large scale polarization U and Q data. To show the intrinsic polarized emission from the SNRs, we subtracted a hyper-plane defined by values at the four corners of the U and Q images of the SNRs extracted from the survey. We then re-calculated PI and PA.

Polarized emission at $\lambda 6$ cm was detected from 25 small SNRs. Their images are shown in Fig. 3 except for Cas A. The integrated polarization flux density and the average polarization percentage were also estimated. For SNRs G67.7+1.8 and G76.9+1.0, intrinsic polarized emission could not be separated from the surroundings. The results for the remaining SNRs are listed in Table 2 except for Cas A. Note that the 9.5 beam mostly covers a significant fraction of the SNRs, which may cause beam depolarization. Therefore, the measured values should be considered as lower limits. The polarization percentages that we derived for some objects are definitely small compared to the results obtained with a smaller beam, for example 13% against 32% for G30.7+0.1 (Reich et al. 1986), 5% compared to 24% for DA 495 (Kothes et al. 2008), and 1% versus 6% for G73.9+0.9 (Reich et al. 1986). This can be ascribed to beam depolarization.

It is for the first time that polarized emission was detected from SNRs G16.2–2.7, G69.7+1.0, G84.2–0.8, and G85.9–0.6. SNRs G84.2–0.8 and G85.9–0.6 are probably located behind the H II complex W 80 (Kothes et al. 2001; Uyaniker et al. 2003). It is therefore difficult to observe their polarization at lower frequencies such as 1.4 GHz. The detection of polarization from these objects finally confirms them as SNRs.

In case there were early polarization measurements with single dishes at $\lambda 6$ cm for the SNRs, such as G21.8–0.6 by Kundu et al. (1974), G30.7+1.0 and G73.9+0.9 by Reich et al. (1986), G36.6–0.7 by Fürst et al. (1987), G65.7+1.2 (DA 495) by Kothes et al. (2008), and G182.4+4.3 by Kothes et al. (1998), their polarization morphologies are quite similar compared to

Table 2. Integrated polarized flux density and average percentage polarization for 22 SNRs at $\lambda 6$ cm observed with a 9.5 beam.

SNR	$S_{PI,6\text{cm}}$ (mJy)	S_{PI}/S_I (%)
G16.2–2.7	150±14	12
G21.8–0.6	790±50	3
G30.7+1.0	370±22	13
G34.7–0.4	5000±255	4
G36.6–0.7	365±28	-
G39.2–0.3	240±15	3
G46.8–0.3	595±32	8
G53.6–2.2	220±15	6
G54.4–0.3	795±41	-
G65.7+1.2	87±20	5
G69.7+1.0	27±5	4
G73.9+0.9	70±7	1
G74.9+1.2	334±30	5
G84.2–0.8	464±45	-
G85.9–0.6	130±10	-
G94.0+1.0	170±17	3
G109.1–1.0	212±20	2
G113.0+0.2	491±50	27
G116.9+0.2	503±50	14
G120.1+1.4	275±30	1
G130.7+3.1	1924±200	6
G180.2+4.3	139±14	53

Notes. In cases where the total integrated intensity could not be measured because of confusion no average percentage polarization could be given.

what we obtained, for example the bipolar magnetic field structure of DA 495.

RMs for some SNRs were obtained in the case that polarization observations at other wavelengths were available. To illustrate this we take the sources G34.7–0.4 (W44) and G116.9+0.2 (CTB 1). W 44 shows a complex pattern in its polarization angle distribution. We retrieved polarization data from the Effelsberg $\lambda 11$ cm polarization survey (Junkes et al. 1987; Duncan et al. 1999) and compared them with the present $\lambda 6$ cm map. The RM is estimated to be about -55 rad m^{-2} and -105 rad m^{-2} towards the southern ($b < -0.5$) and northern ($b > -0.5$) parts of W 44, respectively. The pulsar PSR J1856+0113 ($l = 34.56^\circ$, $b = -0.5^\circ$) associated with W 44 has a RM of $-140 \pm 30 \text{ rad m}^{-2}$ (Han et al. 2006), which is roughly consistent with our estimate. CTB 1 is an evolved SNR. The B-vectors follow the shell at 10.6 GHz (Reich 2002) and deviate by about 40° from the shell at $\lambda 6$ cm. According to these data we calculated a RM of about -180 rad m^{-2} in the western shell.

RMs can also be estimated for some shell-type SNRs based on the morphology by assuming that the intrinsic magnetic field is tangential (e.g. Reich 2002), such as G54.4–0.3 (HC 40). This SNR shows B-vectors that deviate significantly from the shell direction, which indicates an RM of about $250 \pm 100 \text{ rad m}^{-2}$.

3.4. G16.8–1.1 is an HII region

A flat spectrum with $\alpha \sim 0.16$ was earlier derived by Reich et al. (1986), which in principle could indicate either a thermal source or a crab-like SNR. Reich et al. (1986) classified it as a SNR, because strong polarized emission was observed with the Effelsberg 100-m telescope at $\lambda 6$ cm resulting in a percentage polarization of about 15%. The slightly inverted spectrum was thought to be influenced by the compact H II region Sh 2-50 coinciding with the SNR. It should be in front of

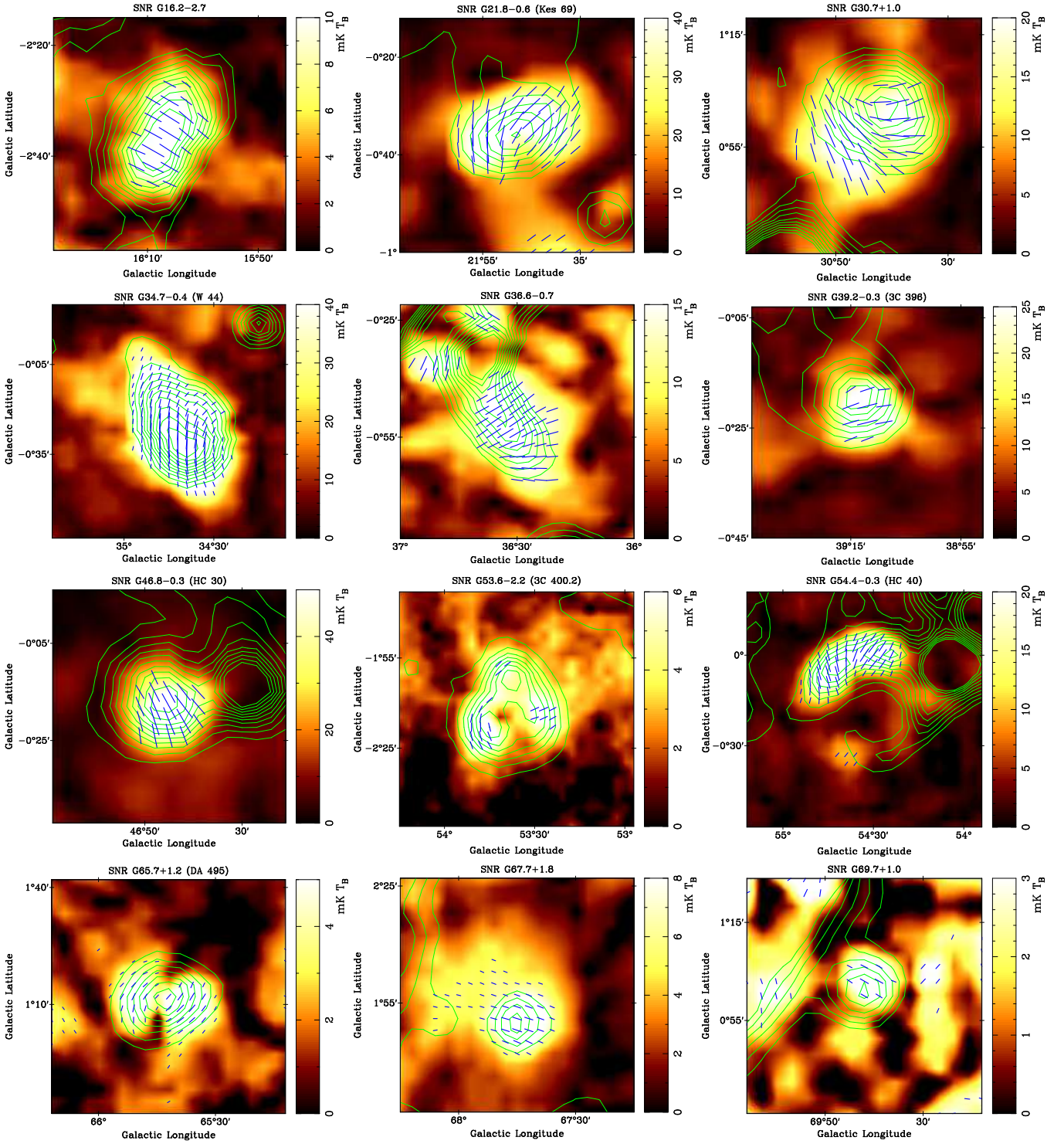


Fig. 3. $\lambda 6$ cm images of SNRs. Polarized intensity is encoded in images, while contours show total intensities. Bars indicate B-vectors (observed E-vectors + 90°). The starting levels and the contour step intervals (both in $\text{mK } T_B$) are for G16.2–2.7: 20 and 6, for G21.8–0.6: 800 and 250, for G30.7+1.0: 10 and 15, for G34.7–0.4: 500 and 300, for G36.6–0.7: 20 and 10, for G39.2–0.3: 250 and 150, for G46.8–0.3: 50 and 50, for G53.6–2.2: 6 and 15, for G54.4–0.3: 50 and 20, for G65.7+1.2: 30 and 15, for G67.7+1.8: 5 and 8, and for G69.7+1.0: 30 and 8.

G16.8–1.1, because it causes depolarization. The pulsar PSR B1822–14 (Clifton & Lyne 1986) is seen within the area of G16.8–1.1 showing a very high RM of -899 rad m^{-2} . Its relation to G16.8–1.1 is still unclear.

The $0.5^\circ \times 0.5^\circ$ Effelsberg map presented by Reich et al. (1986) covers G16.8–1.1, but does not show its surroundings. On a

larger $2^\circ \times 2^\circ$ map (Fig. 4, top panel) extracted from the new $\lambda 6$ cm survey, strong polarization intensity in the surrounding area of G16.8–1.1 is also visible. The central area of the source, however, seems to be nearly unpolarized. The edge areas of the smaller Effelsberg $\lambda 6$ cm map (Reich et al. 1986) almost coincide with strong polarized emission (Fig. 4) as visible in the

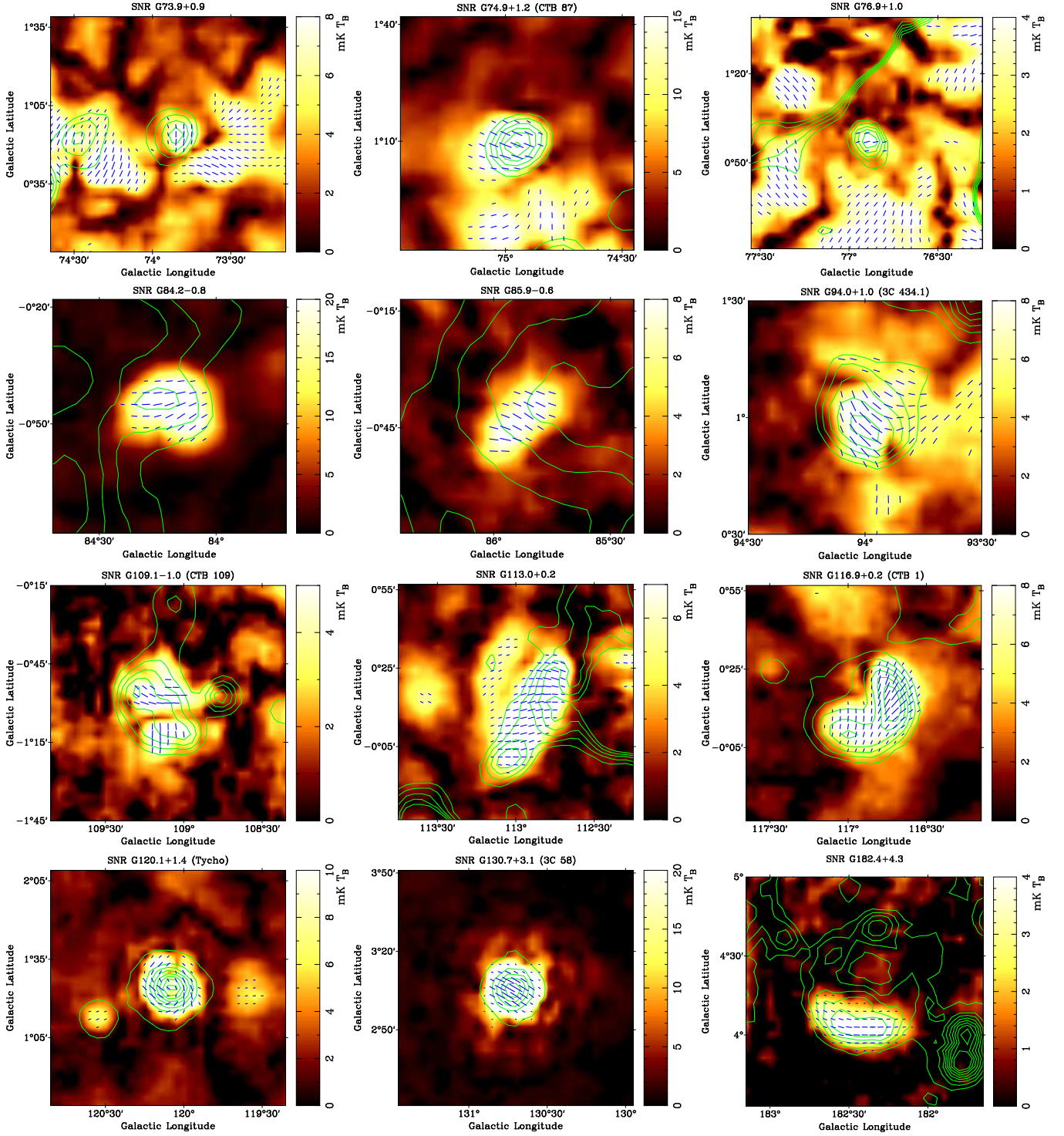


Fig. 3. –continued. The starting levels and the contour step intervals (both in mK T_B) are for G73.9+0.9: 250 and 50, for G74.9+1.2: 250 and 100, for G76.9+1.0: 65 and 10, for G84.2-0.8: 400 and 100, for G85.9-0.6: 200 and 100, for G94.0+1.0: 120 and 30, for G109.1-1.0: 100 and 50, for G113.0+0.2: 30 and 8, for G116.9+0.2: 35 and 15, for G120.1+1.4: 50 and 300, for G130.7+3.1: 100 and 800, and for G182.4+4.3: 2 and 2.

Urumqi $\lambda 6$ cm survey. Standard baseline subtraction assumes zero emission at the edges of a map. If this assumption does not hold, the polarized emission level in a map is not correct. Thus the main argument for a SNR identification of G16.8-1.1 becomes questionable and the entire G16.8-1.1 complex might be considered as thermal. Actually the $\lambda 6$ cm total intensity of G16.8-1.1 fairly well matches the H α emission (Finkbeiner

2003) from the HII region Sh 2-50 (Fig. 4, middle panel), indicating that they are probably the same object.

To check whether G16.8-1.1 acts as a Faraday screen (e.g. Sun et al. 2007; Gao et al. 2010), we show the $\lambda 6$ cm polarization intensity with large-scale emission restored according to WMAP data (Sun et al. 2011) in the bottom panel in Fig. 4. There is indication of insignificant rotation of polarization angles

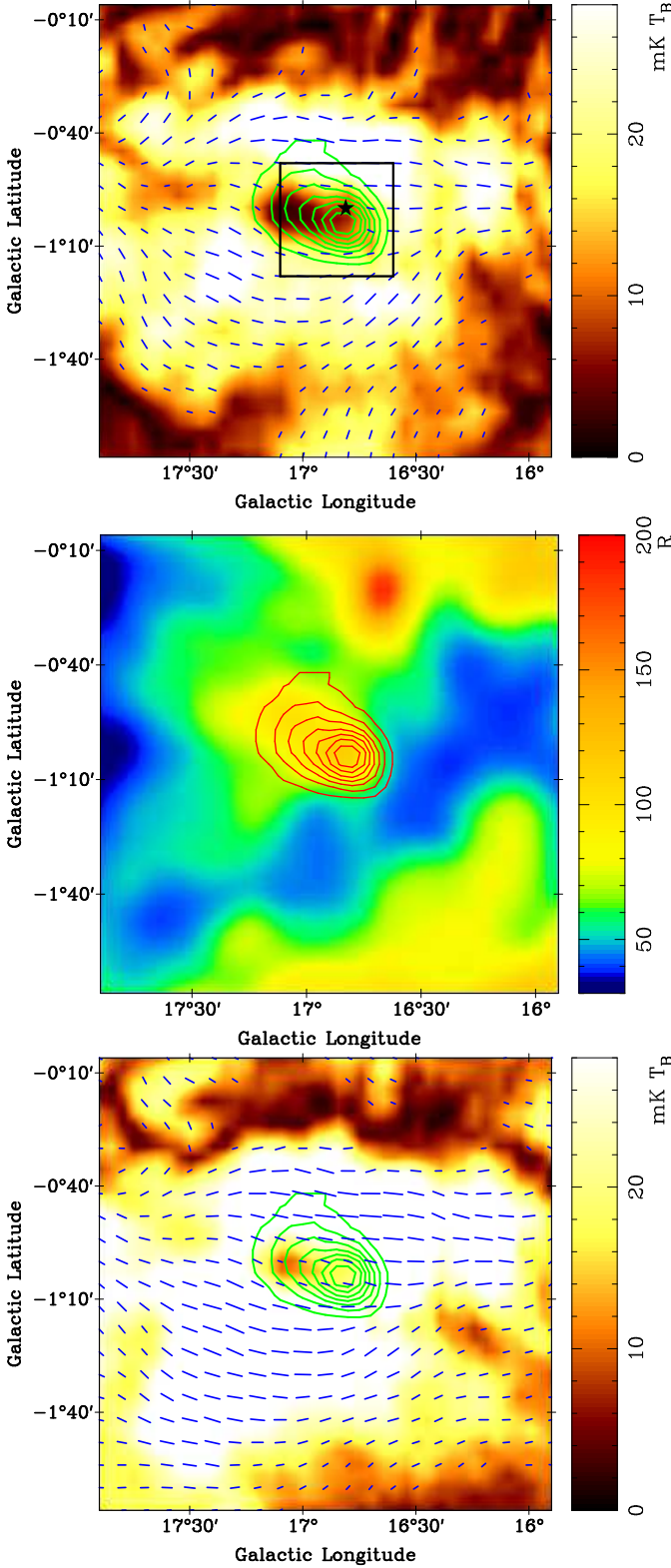


Fig. 4. Images of G16.8–1.1. The contours display the total intensity at $\lambda 6$ cm, starting at 50 mK T_B and running in steps of 50 mK T_B . The image shows the observed $\lambda 6$ cm polarization intensity in the *top* panel, the $H\alpha$ intensity in the *middle* panel, and the absolutely calibrated $\lambda 6$ cm polarization intensity in the *bottom* panel. The bars indicate B-vectors with their lengths proportional to polarized intensity with a low intensity cutoff of 1 mK T_B . The box indicates the mapped region by Reich et al. (1986). The star indicates the position of the pulsar PSR B1822–14.

but some depolarization towards G16.8–1.1, which suggests that G16.8–1.1 is either within the polarized emission region or at a smaller distance than the polarized emission. More data are needed to settle this relation. Sh 2-50 is probably associated with the Scutum super shell at a distance of about 3.3 kpc (Callaway et al. 2000), which is close to the polarization horizon at $\lambda 6$ cm as discussed by Sun et al. (2011).

In case that G16.8–1.1 is thermal, the distance of 5.1 kpc to the pulsar PSR B1822–14, based on the NE2001 model, will be reduced. Its large negative RM might be affected by G16.8–1.1 in a way already described by Mitra et al. (2003) for pulsars shining through H II regions.

3.5. Cas A

Cas A is the strongest radio source seen beyond the solar system and included in the $\lambda 6$ cm survey section presented by Xiao et al. (2011). The Cas A area was observed several times between 2004 and 2008. The peak brightness temperature at $\lambda 6$ cm is around 95 K. For this large intensity, we have checked that the linearity of the receiving system holds.

Cas A is a young SNR whose intensity shows a secular decrease with the rate determined by Baars et al. (1977) as

$$\frac{dS}{S dt} = \left[(0.97 \pm 0.04) - (0.30 \pm 0.04) \lg \left(\frac{\nu}{\text{GHz}} \right) \right] \% \text{ yr}^{-1}. \quad (1)$$

At 4.8 GHz the decreasing rate is 0.77% per year. The absolute spectrum for Cas A was also determined by Baars et al. (1977). In epoch 1965.0, the spectral index $\alpha = -0.792$ between 0.3 GHz and 31 GHz and the flux density at 4.8 GHz is 921.4 Jy. The expected flux density at $\lambda 6$ cm in epoch 2004 is 684 ± 18 Jy and in epoch 2008 is 663 ± 19 Jy. The measured flux density at $\lambda 6$ cm is 688 ± 35 Jy, which agrees with the expectations based on Baars et al. (1977) within the errors. We note that Hafez et al. (2008) proposed a lower decrease rate for Cas A based on new observations as

$$\frac{dS}{S dt} = \left[(0.68 \pm 0.04) - (0.15 \pm 0.04) \lg \left(\frac{\nu}{\text{GHz}} \right) \right] \% \text{ yr}^{-1}. \quad (2)$$

Applying Eq. (2) we calculated a decrease rate of 0.58% at $\lambda 6$ cm, resulting in a flux density of 736 ± 20 Jy in epoch 2004 and 718 ± 21 Jy in epoch 2008. These values are somewhat larger than what we measured.

Cas A has a size of about $5'$ and cannot be resolved in the $\lambda 6$ cm survey. As a very young shell-type SNR the magnetic field is expected to be radial. This can be seen from Effelsberg 32 GHz observations, which resolve Cas A (Reich 2002). We measured a polarization flux density at $\lambda 6$ cm of 38 ± 4 Jy for this SNR, corresponding to an average polarization percentage of about 6%.

4. Summary

We studied small SNRs with angular sizes less than 1° in the Sino-German $\lambda 6$ cm polarization survey of the Galactic plane. Integrated flux densities of 51 SNRs were obtained. Fitting these measurements together with previous observations at other wavelengths, we obtained spectra of 50 SNRs. For half of the SNRs, the $\lambda 6$ cm measurements provide by far the highest frequency data, and therefore play an important role on constraining the spectra of these SNRs. We have determined spectra for SNRs G15.1–1.6, G16.2–2.7, G16.4–0.5, G17.4–2.3, G17.8–2.6, G20.4+0.1, G36.6+2.6, G43.9+1.6, G53.6–2.2,

G55.7+3.4, G59.8+1.2, G68.6–1.2, and G113.0+0.2, by mainly using the flux densities from the $\lambda 6$ cm survey, along with the $\lambda 11$ cm and $\lambda 21$ cm Effelsberg surveys. Note that spectra of these SNRs were poorly determined up to present. G16.8–1.1 is most likely an H II region and not a SNR.

We were also able to extract polarization images of 25 SNRs. For SNRs G16.2–2.7, G69.7+1.0, G84.2–0.8, and G85.9–0.6, the polarized emission is detected for the first time. For some SNRs, RMs could be estimated.

We conclude that it is important to observe SNRs at high frequencies to accurately determine their spectra and study their intrinsic polarization properties.

Acknowledgements. We like to thank the staff of the Urumqi Observatory for qualified assistance during the installation of the receiving system and the survey observations. In particular we are grateful to Otmar Lochner for the construction of the $\lambda 6$ cm receiver, installation and commissioning. Maozheng Chen and Jun Ma helped with the installation of the $\lambda 6$ cm receiving system and maintained it since 2004. We thank Prof. Ernst Fürst for his support of the survey project and critical reading of the manuscript. The MPG and the NAOC supported the construction of the Urumqi $\lambda 6$ cm receiving system by special funds. The Chinese survey team is supported by the National Natural Science Foundation of China (10773016, 10833003, 10821061) and the National Key Basic Research Science Foundation of China (2007CB815403). XHS acknowledges financial support by the MPG and by Prof. Michael Kramer during his stay at MPIfR Bonn. Some data in this paper are based on observations with the 100-m telescope of the MPIfR at Effelsberg. XYG is supported by the Young Researcher Grant of NAOC. We thank the anonymous referee for the very helpful comments which has significantly improved the paper.

References

- Altenhoff, W. J., Downes, D., Goad, L., Maxwell, A., & Rinehart, R. 1970, *A&AS*, 1, 319
- Altenhoff, W. J., Downes, D., Pauls, T., & Schraml, J. 1979, *A&AS*, 35, 23
- Angerhofer, P. E., Becker, R. H., & Kundu, M. R. 1977, *A&A*, 55, 11
- Baars, J. W. M., Genzel, R., Pauliny-Toth, I. I. K., & Witzel, A. 1977, *A&A*, 61, 99
- Barnes, P. J., & Turtle, A. J. 1988, in *IAU Colloq. 101: Supernova Remnants and the Interstellar Medium*, ed. R. S. Roger & T. L. Landecker, 347
- Beard, M., & Kerr, F. J. 1969, *AuJP*, 22, 121
- Becker, R. H., & Kundu, M. R. 1975, *AJ*, 80, 679
- Becker, R. H., & Kundu, M. R. 1976, *ApJ*, 204, 427
- Becker, R. H., & Helfand, D. J. 1985, *ApJ*, 297, L25
- Becker, R. H., & Helfand, D. J. 1987, *AJ*, 94, 1629
- Becker, R. H., White, R. L., & Edwards, A. L. 1991, *ApJS*, 75, 1
- Bennett, A. S. 1962, *MmRAS*, 68, 163
- Bietenholz, M. F., Kassim, N. E., & Weiler, K. W. 2001, *ApJ*, 560, 772
- Binette, L., Carignan, C., Bolton, J. C., & Wright, A. E. 1981, *AuJP*, 34, 407
- Bock, D., Wright, M. C. H., & Dickel, J. R. 2001, *ApJ*, 561, L203
- Boumis, P., Mavromatakis, F., Xilouris, E. M., et al. 2005, *A&A*, 443, 175
- Boumis, P., Alikakos, J., Christopoulou, P. E., et al. 2008, *A&A*, 481, 705
- Bridle, A. H., & Kesteven, M. J. L. 1971, *AJ*, 76, 958
- Brogan, C. L., Lazio, T. J., Kassim, N. E., & Dyer, K. K. 2005, *AJ*, 130, 148
- Brogan, C. L., Gelfand, J. D., Gaensler, B. M., Kassim, N. E., & Lazio, T. J. W. 2006, *ApJ*, 639, L25
- Callaway, M. B., Savage, B. D., Benjamin, R. A., Haffner, L. M., & Tufte, S. L. 2000, *ApJ*, 532, 943
- Castelletti, G., Dubner, G., Brogan, C., & Kassim, N. E. 2007, *A&A*, 471, 537
- Caswell, J. L., Dulk, G. A., Goss, W. M., Radhakrishnan, V., & Green, A. J. 1971, *A&A*, 12, 271
- Caswell, J. L., Clark, D. H., & Crawford, D. F. 1975, *AuJPAS*, 37, 39
- Caswell, J. L., Landecker, T. L., & Feldman, P. A. 1985, *AJ*, 90, 488
- Caswell, J. L., & Haynes, R. F. 1987, *A&A*, 171, 261
- Chaisson, E. J. 1974, *ApJ*, 189, 69
- Clark, D. H., & Crawford, D. F. 1974, *AuJP*, 27, 713
- Clark, D. H., Caswell, J. L., & Green, A. J. 1975a, *AuJPAS*, 37, 1
- Clark, D. H., Green, A. J., & Caswell, J. L. 1975b, *AuJPAS*, 37, 75
- Clifton, T. R., & Lyne, A. G. 1986, *Nature*, 320, 43
- Conway, R. G., Daintree, E. J., & Long, R. J. 1965, *MNRAS*, 131, 159
- Davis, M. M., Gelato-Volders, L., & Westerhout, G. 1965, *Bull. Astron. Inst. Netherlands*, 18, 42
- Day, G. A., Warne, W. G., & Cooke, D. J. 1970, *AuJPAS*, 13, 11
- Dickel, J. R., Webber, J. C., & Yang, K. S. 1971, *AJ*, 76, 294
- Dickel, J. R., Milne, D. K., Kerr, A. R., & Ables, J. G. 1973, *AuJP*, 26, 379
- Dickel, J. R., & Denoyer, L. K. 1975, *AJ*, 80, 437
- Downes, A. J. B., Salter, C. J., & Pauls, T. 1980a, *A&A*, 92, 47
- Downes, D., Wilson, T. L., Bieging, J., & Wink, J. 1980b, *A&AS*, 40, 379
- Downes, A. J. B., Salter, C. J., & Pauls, T. 1981a, *A&A*, 97, 296
- Downes, A. J. B., Salter, C. J., & Pauls, T. 1981b, *A&A*, 97, 296
- Downes, A. 1983, *MNRAS*, 203, 695
- Dubner, G. M., Giacani, E. B., Goss, W. M., & Winkler, P. F. 1994, *AJ*, 108, 207
- Dubner, G. M., Giacani, E. B., Goss, W. M., Moffett, D. A., & Holdaway, M. 1996, *AJ*, 111, 1304
- Duin, R. M., Israel, F. P., Dickel, J. R., & Seaquist, E. R. 1975, *A&A*, 38, 461
- Dulk, G. A., & Slee, O. B. 1975, *ApJ*, 199, 61
- Duncan, A. R., Reich, P., Reich, W., & Fürst, E. 1999, *A&A*, 350, 447
- Fanti, C., Felli, M., Ficarra, A., et al. 1974, *A&AS*, 16, 43
- Finkbeiner, D. P. 2003, *ApJS*, 146, 407
- Foster, T. 2005, *A&A*, 441, 1043
- Fürst, E., Reich, W., Reich, P., Sofue, Y., & Handa, T. 1985, *Nature*, 314, 720
- Fürst, E., Reich, W., Reich, P., Handa, T., & Sofue, Y. 1987, *A&AS*, 69, 403
- Fürst, E., Reich, W., Reich, P., & Reif, K. 1990, *A&AS*, 85, 691
- Fürst, E., Reich, W., Reich, P., & Reif, K. 1990, *A&AS*, 85, 805
- Gao, X. Y., Reich, W., Han, J. L., et al. 2010, *A&A*, 515, A64
- Gao, X. Y., Han, J. L., Reich, W., et al. 2011, *A&A*, 529, A159
- Gardner, F. F., Morris, D., & Whiteoak, J. B. 1969, *AuJP*, 22, 79
- Gardner, F. F., Whiteoak, J. B., & Morris, D. 1975, *AuJPAS*, 35, 1
- Geldzahler, B. J., Pauls, T., & Salter, C. J. 1980, *A&A*, 84, 237
- Giacani, E. B., Dubner, G. M., Kassim, N. E., et al. 1997, *AJ*, 113, 1379
- Giacani, E., Smith, M. J. S., Dubner, G., et al. 2009, *A&A*, 507, 841
- Goss, W. M., & Day, G. A. 1970, *AuJPAS*, 13, 3
- Goss, W. M., & Shaver, P. A. 1970, *AuJPAS*, 14, 1
- Goss, W. M., Schwarz, U. J., & Siddesh, S. G. 1975, *A&A*, 43, 459
- Goss, W. M., Schwartz, U. J., Siddesh, S. G., & Weiler, K. W. 1977, *A&A*, 61, 93
- Goss, W. M., Shaver, P. A., Skellern, D. J., & Watkinson, A. 1979, *A&A*, 78, 75
- Goss, W. M., Mantovani, F., Salter, C. J., Tomasi, P., & Velusamy, T. 1984, *A&A*, 138, 469
- Gower, J. F. R., Scott, P. F., & Wills, D. 1967, *MmRAS*, 71, 49
- Green, A. J. 1974, *A&AS*, 18, 267
- Green, A. J., Baker, J. R., & Landecker, T. L. 1975, *A&A*, 44, 187
- Green, D. A. 1986, *MNRAS*, 218, 533
- Green, D. A. 2009, *BASI*, 37, 45
- Hafez, Y. A., Davies, R. D., Davis, R. J., et al. 2008, *MNRAS*, 388, 1775
- Han, J. L., Manchester, R. N., Lyne, A. G., Qiao, G. J., & van Straten, W. 2006, *ApJ*, 642, 868
- Harris, D. E. 1962, *ApJ*, 135, 661
- Haslam, C. G. T. 1974, *A&AS*, 15, 333
- Helfand, D. J., Velusamy, T., Becker, R. H., & Lockman, F. J. 1989, *ApJ*, 341, 151
- Holden, D. J., & Caswell, J. L. 1969, *MNRAS*, 143, 407
- Horton, P. W., Conway, R. G., & Daintree, E. J. 1969, *MNRAS*, 143, 245
- Hughes, V. A., & Butler, R. 1969a, *AJ*, 74, 608
- Hughes, V. A., & Butler, R. 1969b, *ApJ*, 155, 1061
- Hughes, V. A., Harten, R. H., Costain, C. H., Nelson, L. A., & Viner, M. R. 1984, *ApJ*, 283, 147
- Hurley-Walker, N., Scaife, A. M. M., Green, D. A., et al. 2009, *MNRAS*, 396, 365
- Junkes, N. 1986, Diploma thesis, Bonn University
- Junkes, N., Fürst, E., & Reich, W. 1987, *A&AS*, 69, 451
- Junkes, N., Fürst, E., & Reich, W. 1988, in *Lecture Notes in Physics*, Berlin Springer Verlag, Vol. 316, *Supernova Shells and Their Birth Events*, ed. W. Kundt, 134
- Kassim, N. E. 1989a, *ApJ*, 347, 915
- Kassim, N. E. 1989b, *ApJS*, 71, 799
- Kassim, N. E. 1992, *AJ*, 103, 943
- Kellermann, K. I., Pauliny-Toth, I. I. K., & Tyler, W. C. 1968, *AJ*, 73, 298
- Kellermann, K. I., Pauliny-Toth, I. I. K., & Williams, P. J. S. 1969, *ApJ*, 157, 1
- Kesteven, M. J. L. 1968, *AuJP*, 21, 369
- Klein, U., Emerson, D. T., Haslam, C. G. T., & Salter, C. J. 1979, *A&A*, 76, 120
- Kothes, R., Fürst, E., & Reich, W. 1998, *A&A*, 331, 661
- Kothes, R., Landecker, T. L., Foster, T., & Leahy, D. A. 2001, *A&A*, 376, 641
- Kothes, R., & Reich, W. 2001, *A&A*, 372, 627
- Kothes, R., Uyaniker, B., & Reid, R. I. 2005, *A&A*, 444, 871
- Kothes, R., Fedotov, K., Foster, T. J., & Uyaniker, B. 2006, *A&A*, 457, 1081
- Kothes, R., Landecker, T. L., Reich, W., Safi-Harb, S., & Arzoumanian, Z. 2008, *ApJ*, 687, 516
- Kundu, M. R., & Velusamy, T. 1969, *ApJ*, 155, 807
- Kundu, M. R., & Velusamy, T. 1972, *A&A*, 20, 237
- Kundu, M. R., Velusamy, T., & Hardee, P. E. 1974, *AJ*, 79, 132
- Kuz'min, A. D., Levchenko, M. T., Noskova, R. I., & Salomonovich, A. E. 1960, *AZh*, 37, 975

- Kuz'min, A. D. 1962, *Soviet Ast.*, 5, 692
- Lacey, C. K., Lazio, T. J. W., Kassim, N. E., et al. 2001, *ApJ*, 559, 954
- Landecker, T. L., Roger, R. S., & Dewdney, P. E. 1982, *AJ*, 87, 1379
- Landecker, T. L., & Caswell, J. L. 1983, *AJ*, 88, 1810
- Landecker, T. L., Higgs, L. A., & Roger, R. S. 1985, *AJ*, 90, 1082
- Landecker, T. L., Higgs, L. A., & Wendker, H. J. 1993, *A&A*, 276, 522
- Landecker, T. L., Zheng, Y., Zhang, X., & Higgs, L. A. 1997, *A&AS*, 123, 199
- Langston, G., Minter, A., D'Addario, L., et al. 2000, *AJ*, 119, 2801
- Large, M. I., Mathewson, D. S., & Haslam, C. G. T. 1961, *MNRAS*, 123, 113
- Leslie, P. R. R. 1960, *The Observatory*, 80, 23
- Mantovani, F., Nanni, M., Salter, C. J., & Tomasi, P. 1982, *A&A*, 105, 176
- Marthi, V. R., Chengalur, J. N., Gupta, Y., Dewangan, G. C., & Bhattacharya, D. 2011, *MNRAS*, in press
- Milne, D. K. 1969, *AuJP*, 22, 613
- Milne, D. K., Wilson, T. L., Gardner, F. F., & Mezger, P. G. 1969, *Astrophys. Lett.*, 4, 121
- Milne, D. K., & Dickel, J. R. 1974, *AuJP*, 27, 549
- Milne, D. K., & Dickel, J. R. 1975, *AuJP*, 28, 209
- Milne, D. K., Caswell, J. L., Kesteven, M. J., Haynes, R. F., & Roger, R. S. 1989, *Proceedings of the Astronomical Society of Australia*, 8, 187
- Mitra, D., Wielebinski, R., Kramer, M., & Jessner, A. 2003, *A&A*, 398, 993
- Moffett, D. A., & Reynolds, S. P. 1994a, *ApJ*, 425, 668
- Moffett, D. A., & Reynolds, S. P. 1994b, *ApJ*, 437, 705
- Moran, M. 1965, *MNRAS*, 129, 447
- Morsi, H. W. 1982, Diploma thesis, Bonn University
- Morsi, H. W., & Reich, W. 1987a, *A&AS*, 69, 533
- Morsi, H. W., & Reich, W. 1987b, *A&AS*, 71, 189
- Odegard, N. 1986, *AJ*, 92, 1372
- Patnaik, A. R., Velusamy, T., & Venugopal, V. R. 1988, *Nature*, 332, 136
- Patnaik, A. R., Hunt, G. C., Salter, C. J., Shaver, P. A., & Velusamy, T. 1990, *A&A*, 232, 467
- Pauliny-Toth, I. I. K., Wade, C. M., & Heeschen, D. S. 1966, *ApJS*, 13, 65
- Pineault, S., & Chastenay, P. 1990, *MNRAS*, 246, 169
- Reich, P., Reich, W., & Fürst, E. 1997, *A&AS*, 126, 413
- Reich, W., & Braunsfurth, E. 1981, *A&A*, 99, 17
- Reich, W., Fürst, E., Haslam, C. G. T., Steffen, P., & Reif, K. 1984a, *A&AS*, 58, 197
- Reich, W., Fürst, E., & Sofue, Y. 1984b, *A&A*, 133, L4
- Reich, W., Fürst, E., Reich, P., Sofue, Y., & Handa, T. 1986, *A&A*, 155, 185
- Reich, W., Fürst, E., Reich, P., & Junkes, N. 1988, in *IAU Colloq. 101: Supernova Remnants and the Interstellar Medium*, ed. R. S. Roger & T. L. Landecker, 293
- Reich, W., Fürst, E., Reich, P., & Reif, K. 1990a, *A&AS*, 85, 633
- Reich, W., Reich, P., & Fürst, E. 1990b, *A&AS*, 83, 539
- Reich, W. 2002, in *Neutron Stars, Pulsars, and Supernova Remnants*, ed. W. Becker, H. Lesch, & J. Trümper, 1
- Reifenstein, E. C., Wilson, T. L., Burke, B. F., Mezger, P. G., & Altenhoff, W. J. 1970, *A&A*, 4, 357
- Salter, C. J., Emerson, D. T., Steppe, H., & Thum, C. 1989a, *A&A*, 225, 167
- Salter, C. J., Reynolds, S. P., Hogg, D. E., Payne, J. M., & Rhodes, P. J. 1989b, *ApJ*, 338, 171
- Scaife, A., Green, D. A., Battye, R. A., et al. 2007, *MNRAS*, 377, L69
- Scheuer, P. A. G. 1963, *The Observatory*, 83, 56
- Shaver, P. A., & Goss, W. M. 1970, *AuJPAS*, 14, 133
- Shaver, P. A., & Weiler, K. W. 1976, *A&A*, 53, 237
- Sieber, W., & Seiradakis, J. H. 1984, *A&A*, 130, 257
- Slee, O. B. 1977, *AuJPAS*, 43, 1
- Sofue, Y., & Reich, W. 1979, *A&AS*, 38, 251
- Sofue, Y., Takahara, F., & Hirabayashi, H. 1983, *PASJ*, 35, 447
- Sun, X. H., Han, J. L., Reich, W., et al. 2007, *A&A*, 463, 993
- Sun, X. H., Reich, W., Han, J. L., et al. 2011, *A&A*, 527, A74
- Tam, C., Roberts, M. S. E., & Kaspi, V. M. 2002, *ApJ*, 572, 202
- Taylor, A. R., Wallace, B. J., & Goss, W. M. 1992, *AJ*, 103, 931
- Taylor, A. R., Goss, W. M., Coleman, P. H., van Leeuwen, J., & Wallace, B. J. 1996, *ApJS*, 107, 239
- Tian, W., & Leahy, D. 2006, *Chinese J. Astron. Astrophys.*, 6, 543
- Trushkin, S. A. 1999, *A&A*, 352, L103
- Turtle, A. J., Pugh, J. F., Kenderdine, S., & Pauliny-Toth, I. I. K. 1962, *MNRAS*, 124, 297
- Uyaniker, B., Landecker, T. L., Gray, A. D., & Kothes, R. 2003, *ApJ*, 585, 785
- Velusamy, T., & Kundu, M. R. 1974, *A&A*, 32, 375
- Vessey, S. J., & Green, D. A. 1998, *MNRAS*, 294, 607
- Wallace, B. J., Landecker, T. L., & Taylor, A. R. 1997a, *AJ*, 114, 2068
- Wallace, B. J., Landecker, T. L., Taylor, A. R., & Pineault, S. 1997b, *A&A*, 317, 212
- Weiler, K. W., & Shaver, P. A. 1978, *A&A*, 70, 389
- Wendker, H. J., Higgs, L. A., & Landecker, T. L. 1991, *A&A*, 241, 551
- Westerhout, G. 1958, *Bull. Astron. Inst. Netherlands*, 14, 215
- White, R. L., & Becker, R. H. 1992, *ApJS*, 79, 331
- Willis, A. G. 1973, *A&A*, 26, 237
- Wilson, R. W. 1963, *AJ*, 68, 181
- Wilson, A. S., & Weiler, K. W. 1976, *A&A*, 53, 89
- Xiao, L., Han, J. L., Reich, W., et al. 2011, *A&A*, 529, A15

Table 1. SNRs with flux densities measured from the $\lambda 6$ cm survey.

Name	Prev. $S_{6\text{cm}}$ (Jy)	Ref.	New $S_{6\text{cm}}$ (Jy)	Prev. α	Ref.	New α	Ref.
G11.1–1.0	5.6±0.6	3	3.40±0.25	–0.6	2	–0.41±0.02	1–5
G11.2–0.3	9.6±0.5	11	8.95±0.48	–0.50±0.02	11	–0.48±0.01	1, 4, 5, 6–19
G15.1–1.6	4.81±0.27	–0.8?	142	–0.01±0.09	1, 4
G15.4+0.1	2.07±0.18	–0.6	2	–0.62±0.03	1, 2
G15.9+0.2	1.9±0.2	21	1.95±0.29	–0.63	22	–0.63±0.03	1, 4, 5, 8, 14, 16, 20–22
G16.2–2.7	1.28±0.10	–0.51±0.10	23	–0.42±0.10	23
G16.4–0.5	2.97±0.26	–0.7	2	–0.26±0.15	2
G16.7+0.1	0.95±0.10	24	1.23±0.11	–0.6	24	–0.56±0.05	1, 5, 14, 24
G16.8–1.1	7.4±1.2	25	7.39±0.39	0.16	25	0.25±0.07	1, 5, 25
G17.4–2.3	2.33±0.23	–0.8?	142	–0.46±0.12	4
G17.8–2.6	2.28±0.13	–0.3?	142	–0.50±0.07	
G18.8+0.3	15.7±3	31	15.29±0.89	–0.42	22	–0.46±0.02	1, 4, 8, 10, 15, 22, 26–32
G18.9–1.1	23.8±2.4	34	19.57±1.01	–0.4	34	–0.39±0.03	1, 4, 33–35
G20.0–0.2	10.4±1	36	9.23±0.54	–0.04±0.06	143	–0.06±0.04	1, 4, 5, 14, 36
G20.4+0.1	7.50±0.50	–0.4	2	–0.08±0.09	2, 4
G21.5–0.9	7.2±1	45	6.54±0.37	0.0	42	–0.06±0.03	1, 4–6, 10, 13, 15, 28, 37–45
						–0.41±0.09	
G21.8–0.6	29±3	9	24.03±1.29	–0.5	10	–0.56±0.03	1, 4, 8–10, 13, 15, 17, 30, 32, 41, 46, 47
G27.8+0.6	18±2	48	20.98±1.08	–0.3±0.1	48	–0.25±0.07	1, 48
G29.7–0.3	3.4±0.7	31	3.62±0.58	–0.66	12	–0.63±0.02	1, 6–8, 10, 12, 16–18, 27, 31, 40, 41, 49, 50
G30.7+1.0	3.4±0.4	25	2.93±0.19	–0.34	25	–0.38±0.05	10, 25
G31.9+0.0	10±1	31	8.94±0.56	–0.5	63	–0.02±0.04	1, 5–8, 10, 14–16, 27, 31, 49–64
						–0.54±0.02	
G33.6+0.1	11.4±1.1	20	9.44±0.54	–0.4	10	–0.51±0.02	1, 5–8, 10, 14, 16, 20, 52, 65–69
G34.7–0.4	127±13	1	117.55±6.00	–0.37±0.02	70	–0.37±0.02	1, 8, 10, 26, 27, 31, 32, 41, 47, 51, 52, 60, 62, 64, 66, 70–84
G36.6+2.6	0.39±0.04	–0.5?	142	–0.67±0.12	
G39.2–0.3	8.7±0.9	86	8.84±0.53	0.42±0.02	91	–0.34±0.01	1, 5–8, 10, 13–18, 30, 49, 51, 62, 64, 66, 68, 85–92
G40.5–0.5	6.39±0.34	0.41±0.05	93	–0.41±0.08	1, 28, 64, 93, 94
G41.1–0.3	15±1.5	1	18.52±1.07	–0.48	12	–0.50±0.01	1, 5, 7, 8, 10, 12, 14–16, 32, 47, 56, 60, 62, 64–66, 89, 94
G43.3–0.2	17±2	9	19.10±0.98	–0.48	12	–0.46±0.01	1, 7–9, 12, 14, 16, 17, 94–98
G43.9+1.6	4.55±0.24	0.0?	142	–0.47±0.06	
G46.8–0.3	7.1±0.7	65	7.02±0.18	–0.53	22	–0.54±0.02	1, 8, 20, 22, 28, 32, 60, 65, 89, 98
G53.6–2.2	4.00±0.22	–0.76±0.02	99	–0.50±0.02	26, 32, 47, 60, 62, 64, 66, 99, 100
G55.7+3.4	0.52±0.03	–0.6±0.1	101	–0.34±0.11	101
G57.2+0.8	0.62±0.06	102	0.74±0.04	–0.67	104	–0.62±0.01	5, 14, 98, 102–107
G59.8+1.2	1.43±0.08	–0.5	142	–0.03±0.05	
G63.7+1.1	1.16±0.10	108	1.12±0.06	–0.30	104	–0.24±0.02	5, 14, 98, 102, 104, 106, 108
G65.7+1.2	1.79±0.1	111	1.95±0.10	–0.59	111	–0.57±0.01	1, 5, 32, 66, 98, 107, 109–112
G67.7+1.8	0.42±0.05	98	0.30±0.03	–0.49±0.05	110	–0.61±0.01	5, 98, 104, 110
G68.6–1.2	0.80±0.04	0.0?	142	–0.22±0.09	110
G69.7+1.0	0.58±0.05	113	0.68±0.07	–0.70±0.06	110	–0.71±0.05	5, 110, 113, 114
G73.9+0.9	6.7±0.5	25	6.17±0.34	–0.23±0.03	110	–0.23±0.03	5, 25, 110, 115
G74.9+1.2	7.5±0.7	119	6.35±0.35	–0.29±0.02	110	–0.26±0.02	5, 15, 28, 42, 49, 66, 98, 104, 110, 115–121
						–0.71±0.18	
G76.9+1.0	0.63±0.03	122	0.79±0.07	–0.60±0.02	110	–0.89±0.02	5, 40, 98, 104, 110, 122–124
G94.0+1.0	7.2±0.5	126	6.23±0.35	–0.48±0.02	110	–0.45±0.02	32, 47, 51, 62, 64, 110, 125–129
G96.0+2.0	0.14±0.02	–0.45±0.13	110	–0.59±0.07	110
G109.1–1.0	9.78±0.52	–0.50±0.04	110	–0.45±0.04	110, 130–132
G113.0+0.2	1.85±0.50	–0.45±0.25	
G116.9+0.2	3.0±0.3	20	3.60±0.40	–0.61±0.03	110	–0.57±0.03	20, 32, 47, 110, 133–135
G120.1+1.4	21.1±0.4	62	20.03±2.00	–0.65±0.01	110	–0.58±0.02	28, 40, 49, 51, 56, 61, 62, 64, 78, 94, 102, 104, 107, 110, 136–138
G130.7+3.1	31.2±1.8	136	31.66±3.00	–0.07±0.01	110	–0.07±0.02	8, 28, 40, 42, 44, 49, 61, 62, 64, 78, 94, 102, 104, 107, 110, 136, 138–140
G182.4+4.3	0.20±0.02	141	0.26±0.05	–0.44±0.10	141	–0.41±0.14	141

- References.** (1) Altenhoff et al. (1970), (2) Brogan et al. (2006), (3) Caswell & Haynes (1987), (4) Goss & Day (1970), (5) Reich et al. (1990b), (6) Becker & Kundu (1975), (7) Dulk & Slee (1975), (8) Green (1974), (9) Goss & Shaver (1970), (10) Kassim (1992), (11) Kothes & Reich (2001), (12) Morsi & Reich (1987b), (13) Milne et al. (1969), (14) Reich et al. (1984a), (15) Reifstein et al. (1970), (16) Slee (1977), (17) Shaver & Goss (1970), (18) Shaver & Weiler (1976), (19) Tam et al. (2002), (20) Angerhofer et al. (1977), (21) Clark et al. (1975a), (22) Dubner et al. (1996), (23) Trushkin (1999), (24) Helfand et al. (1989), (25) Reich et al. (1986), (26) Clark et al. (1975b), (27) Kesteven (1968), (28) Langston et al. (2000), (29) Milne et al. (1989), (30) Milne & Dickel (1975), (31) Milne (1969), (32) Willis (1973), (33) Barnes & Turtle (1988), (34) Fürst et al. (1985), (35) Patnaik et al. (1988), (36) Becker & Helfand (1985), (37) Becker & Kundu (1976), (38) Bock et al. (2001), (39) Clark & Crawford (1974), (40) Fürst et al. (1990), (41) Milne & Dickel (1974), (42) Morsi & Reich (1987a), (43) Salter et al. (1989a), (44) Salter et al. (1989b), (45) Wilson & Weiler (1976), (46) Kundu et al. (1974), (47) Velusamy & Kundu (1974), (48) Reich et al. (1984b), (49) Fanti et al. (1974), (50) Gower et al. (1967), (51) Bennett (1962), (52) Beard & Kerr (1969), (53) Bridle & Kesteven (1971), (54) Brogan et al. (2005), (55) Caswell et al. (1971), (56) Conway et al. (1965), (57) Chaisson (1974), (58) Dickel et al. (1973), (59) Goss et al. (1979), (60) Holden & Caswell (1969), (61) Kellermann et al. (1968), (62) Kellermann et al. (1969), (63) Moffett & Reynolds (1994a), (64) Pauliny-Toth et al. (1966), (65) Caswell et al. (1975), (66) Dickel & Denoyer (1975), (67) Gardner et al. (1969), (68) Gardner et al. (1975), (69) Giacani et al. (2009), (70) Castelletti et al. (2007), (71) Davis et al. (1965), (72) Downes et al. (1980b), (73) Giacani et al. (1997), (74) Harris (1962), (75) Kuz'min et al. (1960), (76) Kuz'min (1962), (77) Kundu & Velusamy (1969), (78) Kundu & Velusamy (1972), (79) Large et al. (1961), (80) Leslie (1960), (81) Moran (1965), (82) Scheuer (1963), (83) Westerhout (1958), (84) Wilson (1963), (85) Altenhoff et al. (1979), (86) Binette et al. (1981), (87) Becker & Helfand (1987), (88) Downes et al. (1981a), (89) Day et al. (1970), (90) Hughes & Butler (1969b), (91) Patnaik et al. (1990), (92) Scaife et al. (2007), (93) Downes et al. (1980a), (94) Downes et al. (1981b), (94) Green et al. (1975), (95) Hughes & Butler (1969a), (96) Lacey et al. (2001), (97) Moffett & Reynolds (1994b), (98) Taylor et al. (1992), (99) Dubner et al. (1994), (100) Goss et al. (1975), (101) Goss et al. (1977), (102) Becker et al. (1991), (103) Caswell et al. (1985), (104) Hurley-Walker et al. (2009), (105) Sieber & Seiradakis (1984), (106) Taylor et al. (1996), (107) White & Becker (1992), (108) Wallace et al. (1997a), (109) Dickel et al. (1971), (110) Kothes et al. (2006), (111) Kothes et al. (2008), (112) Landecker & Caswell (1983), (113) Junkes (1986), (114) Junkes et al. (1988), (115) Pineault & Chastenay (1990), (116) Duin et al. (1975), (117) Geldzahler et al. (1980), (118) Morsi (1982), (119) Wendker et al. (1991), (120) Wallace et al. (1997b), (121) Weiler & Shaver (1978), (122) Landecker et al. (1993), (123) Landecker et al. (1997), (124) Marthi et al. (2011), (125) Foster (2005), (126) Goss et al. (1984), (127) Landecker et al. (1985), (128) Mantovani et al. (1982), (129) Vessey & Green (1998), (130) Downes (1983), (131) Hughes et al. (1984), (132) Sofue et al. (1983), (133) Landecker et al. (1982), (134) Reich & Braunsfurth (1981), (135) Tian & Leahy (2006), (136) Horton et al. (1969), (137) Klein et al. (1979), (138) Reich et al. (1997), (139) Bietenholz et al. (2001), (140) Green (1986), (141) Kothes et al. (1998), (142) Reich et al. (1988), (143) Odegard (1986)